Electronic structure of $In_yGa_{1-y}As_{1-x}N_x/GaAs(N)$ quantum dots by ten-band k·p theory

Stanko Tomić
Computational Science and Engineering Department, CCLRC Daresbury Laboratory, Warrington, Cheshire WA4 4AD, United Kingdom
(Received 26 October 2005; revised manuscript received 13 February 2006; published 31 March 2006)

We present a theoretical study of the electronic and optical properties of InGaAsN/GaAs quantum dot structures. The calculations are based on a 10×10 **k**·**p** band anticrossing Hamiltonian, incorporating valence, conduction, and nitrogen-induced bands. Numerical results for the model system of a capped pyramid-shaped quantum dot with {101} facets on a thin wetting layer are presented. Theoretical results show lowering of the fundamental optical transition on introduction of nitrogen. With appropriate tailoring of the indium and nitrogen concentration this system could be a potential candidate for 1.55 μm emission on a GaAs substrate.

DOI: 10.1103/PhysRevB.73.125348 PACS number(s): 73.21.La, 78.67.Hc, 71.20.Nr

I. INTRODUCTION

III-V semiconductor quantum dots (QD) are promising candidates for the active region in the next generation of optoelectronic devices, such as low-chirp lasers,[1] semiconductor optical amplifiers,[2,3] single-photon emitters,[4] or registers in quantum computing.[5] Recent advances in growth techniques facilitate the fabrication of self-assembled QDs with a very small amount ($<4\%$) of nitrogen substitutional impurities in the QD region or in capping layer.[6–11] With appropriate tailoring of the QD morphology, this opens the possibility of GaAs-based optoelectronic devices emitting at 1.55 μm and beyond. It has been found that replacing a small amount of the group V element by nitrogen in a III-V compound reduces the energy gap and increases the electron effective mass in the conduction band. This reduction of energy gap (of $\sim$0.1 eV per percent of N for $x<\sim0.05$) occurs because of a band anticrossing (BAC) interaction between the conduction band edge and a higher-lying nitrogen resonant band[12] and dramatically changes the electronic structure, thus offering a different route to band structure engineering and improved optoelectronic properties.[13] The addition of indium to form $In_yGa_{1-y}As_{1-x}N_x$ has two main effects on the conduction band structure. First, the conduction band edge (CBE) shifts down in energy on an absolute scale with increasing y in $In_yGa_{1-y}As$.[14] Second, because In has a larger atomic radius than Ga, there is a weaker overall lattice perturbation around an isolated N atom bonded to In neighbors, leading to a reduced BAC interaction. There is also a weaker distortion around N-N pairs and other cluster states,[15] which when bonded predominantly to In neighbors consequently lie higher in energy compared to equivalent states in GaAsN.[16] Improved agreement was shown between the electron effective mass predicted by the BAC model and that observed experimentally when there are no cluster states close by in energy with which the InGaAsN CBE can interact.[17,18] This finding justifies that, away from cluster states, the BAC model provides an excellent description not just of the energy gap but also of the band dispersion.

The **k**·**p** and envelope function methods are still widely applied to study III-V semiconductor heterostructures,[19–24] although in recent years, with new computer architectures and increased computational power, calculations that reflect detailed atomistic nature based on pseudopotential method,[25,26] combined with advanced numerical algorithms,[27,28] become feasible methods of nanostructure modeling.

In this paper, we present an initial theoretical analysis of the band structure and optical properties of dilute nitrogen $In_yGa_{1-y}As_{1-x}N_x/GaAs(N)$ quantum dots, using the **k**·**p** theory.

II. THEORETICAL MODEL

The strong interaction between the N resonant states and the conduction band edge means that the conventional eight-band **k**·**p** method cannot be applied directly to (In,Ga)AsN and related heterostructures. The electronic structure is calculated below by extending the conventional eight-band **k**·**p** Hamiltonian[20,21] to a ten-band model.[29] To describe the electronic structure of $In_yGa_{1-y}As_{1-x}N_x$, two (spin-degenerate) nitrogen-related bands were added to the usual two conduction and six valence bands in the conventional eight-band model. Several studies support the idea that the energy of the N resonant state and its coupling to the CBE vary with In composition in $In_yGa_{1-y}As_{1-x}N_x$.[30–32] We assume the N resonant level varies with N and In compositions x and y as $E_{N0}(\mathrm{eV})=1.65-0.18y$, where the zero of energy is taken at the GaAs valence band maximum. The host material unperturbed conduction band energy is assumed to vary with N composition x as $E_{c0}(y)-\alpha x$, with α (in electron volts) $=1.55-0.14y$, while the matrix element linking the N state and the host material CBE is presumed to vary with N composition x and In composition y as[18,32] $V_{Nc0}(\mathrm{eV})=-(2.45-1.17y)\sqrt{x}$. The variant of the ten-band Hamiltonian $H_{\mathbf{k}}$ is derived in the angular momentum Bloch basis

$$|u_1\rangle=\left|\frac{1}{2},+\frac{1}{2}\right\rangle=|s_N;\uparrow\rangle$$

$$|u_2\rangle=\left|\frac{1}{2},+\frac{1}{2}\right\rangle=|s_c;\uparrow\rangle$$

$$|u_3\rangle=\left|\frac{3}{2},+\frac{3}{2}\right\rangle=\frac{i}{\sqrt{2}}[|x;\uparrow\rangle+i|y;\uparrow\rangle]$$

$$|u_4\rangle = \left|\frac{3}{2}, +\frac{1}{2}\right\rangle = \frac{i}{\sqrt{6}}[|x;\downarrow\rangle + i|y;\downarrow\rangle - 2|z;\uparrow\rangle]$$

$$|u_5\rangle = \left|\frac{1}{2}, +\frac{1}{2}\right\rangle = \frac{i}{\sqrt{3}}[|x;\downarrow\rangle + i|y;\downarrow\rangle + |z;\uparrow\rangle].$$

The set of states ($|u_6\rangle - |u_{10}\rangle$) were obtained by application of the time-reversal symmetry operator for zinc-blende structures, $\hat{T}_d = -i\sigma_y \hat{C}\hat{J}$, where σ_y is the Pauli spin matrix, $\hat{C}$ is the complex conjugation operator, and $\hat{J}$ is the inversion about midpoint between nearest neighbors ($s \mapsto -s$, $p \mapsto p$), and reads

$$|u_6\rangle = \left|\frac{1}{2}, -\frac{1}{2}\right\rangle = -|s_N;\downarrow\rangle$$

$$|u_7\rangle = \left|\frac{1}{2}, -\frac{1}{2}\right\rangle = -|s_c;\downarrow\rangle$$

$$|u_8\rangle = \left|\frac{3}{2}, -\frac{3}{2}\right\rangle = -\frac{i}{\sqrt{2}}[|x;\downarrow\rangle - i|y;\downarrow\rangle]$$

$$|u_9\rangle = \left|\frac{3}{2}, -\frac{1}{2}\right\rangle = +\frac{i}{\sqrt{6}}[|x;\uparrow\rangle - i|y;\uparrow\rangle + 2|z;\downarrow\rangle]$$

$$|u_{10}\rangle = \left|\frac{1}{2}, -\frac{1}{2}\right\rangle = +\frac{i}{\sqrt{3}}[|x;\uparrow\rangle - i|y;\uparrow\rangle - |z;\downarrow\rangle].$$

In the absence of external magnetic field, the set of states ($|u_6\rangle - |u_{10}\rangle$) are Kramer's double degenerate to ($|u_1\rangle - |u_5\rangle$).

The strain tensor in the QD (Ref. 33) was determined in analytical form as a solution of the Fourier transform of the lattice displacement Green's function for the crystal with cubic symmetry convoluted with the forces (stress) existing on the surface of the QD.[34] The strain tensor elements were used to form Pikus-Bir Hamiltonian $H_{\mathbf{e}}$, and it takes into account the crystal anisotropy, i.e., $c_{11} - c_{12} - 2c_{14} \neq 0$,[34] where c_{ij} are the elastic constants. From the strain tensor and spatially varying piezoelectric modulus e_{14}, the piezoelectric potential V_{pz} is calculated and included in the final Hamiltonian.

The most general form of the ten-band $\mathbf{k}\cdot\mathbf{p}$ Hamiltonian includes k-dependent diagonal and off-diagonal matrix elements, linking the nitrogen, conduction, and valence basis states

$$\begin{pmatrix}
E_{\mathrm{NB}} & V_{\mathrm{NC}} & -\sqrt{3}T_{\mathrm{N}} & \sqrt{2}U_{\mathrm{N}} & -U_{\mathrm{N}} & 0 & 0 & 0 & -T_{\mathrm{N}}^{*} & -\sqrt{2}T_{\mathrm{N}}^{*} \\
 & E_{\mathrm{CB}} & -\sqrt{3}T & \sqrt{2}U & -U & 0 & 0 & 0 & -T^{*} & -\sqrt{2}T^{*} \\
 & & E_{\mathrm{HH}} & \sqrt{2}S & -S & 0 & 0 & 0 & -R & -\sqrt{2}R \\
 & & & E_{\mathrm{LH}} & -\sqrt{2}Q & T_{\mathrm{N}}^{*} & T^{*} & R & 0 & \sqrt{3}S \\
 & & & & E_{\mathrm{SO}} & \sqrt{2}T_{\mathrm{N}}^{*} & \sqrt{2}T^{*} & \sqrt{2}R & -\sqrt{3}S & 0 \\
 & & & & & E_{\mathrm{NB}} & V_{\mathrm{NC}} & -\sqrt{3}T_{\mathrm{N}}^{*} & \sqrt{2}U_{\mathrm{N}} & -U_{\mathrm{N}} \\
 & & & & & & E_{\mathrm{CB}} & -\sqrt{3}T^{*} & \sqrt{2}U & -U \\
 & & & & & & & E_{\mathrm{HH}} & \sqrt{2}S^{*} & -S^{*} \\
 & & & & & & & & E_{\mathrm{LH}} & -\sqrt{2}Q \\
 & & & & & & & & & E_{\mathrm{SO}}
\end{pmatrix}
\begin{pmatrix}
|u_1\rangle \\ |u_2\rangle \\ |u_3\rangle \\ |u_4\rangle \\ |u_5\rangle \\ |u_6\rangle \\ |u_7\rangle \\ |u_8\rangle \\ |u_9\rangle \\ |u_{10}\rangle
\end{pmatrix}, \tag{1}$$

where diagonal elements are defined as

$$E_{\mathrm{NB}} = E_{\mathrm{N0}} + N + V_{\mathrm{pz}}$$

$$E_{\mathrm{CB}} = E_{c0} + O + V_{\mathrm{pz}}$$

$$E_{\mathrm{HH}} = E_{v0} - (P + Q) + V_{\mathrm{pz}}$$

$$E_{\mathrm{LH}} = E_{v0} - (P - Q) + V_{\mathrm{pz}}$$

$$E_{\mathrm{SO}} = E_{v0} - (P + \Delta_{\mathrm{so}}) + V_{\mathrm{pz}}.$$

The subscripts NB, CB, HH, LH and SO stand for nitrogen resonant, conduction, heavy hole, light hole, and split-off band, respectively, and Δ_{so} is the spin-orbital split-off energy. The unstrained nitrogen resonant (E_{N0}), conduction (E_{c0}), and valence (E_{v0}) band edges, are all aligned relative to the average valence band of the dot or matrix material, respectively.[14,21] The coupling between nitrogen states and the host material conduction band is described by

$$V_{\mathrm{NC}} = V_{\mathrm{Nc0}} + V$$

matrix element. Other Hamiltonian matrix elements are given as a sum of kinetic terms (subscript k) and its strain counterpart (subscript ϵ)

$$N = N_k + N_\epsilon$$

$$O = O_k + O_\epsilon$$

$$P = P_k + P_\epsilon$$

$$Q = Q_k + Q_\epsilon$$

$$R = R_k + R_\epsilon$$

$$S = S_k + S_\epsilon$$

$$T = T_k + T_\epsilon$$

$$U = U_k + U_\epsilon$$

$$V = V_k + V_\epsilon.$$

The kinetic terms are given by

$$N_k = \left(\frac{\hbar^2}{2m_0}\right)\gamma_N(k_x^2 + k_y^2 + k_z^2)$$

$$O_k = \left(\frac{\hbar^2}{2m_0}\right)\gamma_c(k_x^2 + k_y^2 + k_z^2)$$

$$P_k = \left(\frac{\hbar^2}{2m_0}\right)\gamma_1(k_x^2 + k_y^2 + k_z^2)$$

$$Q_k = \left(\frac{\hbar^2}{2m_0}\right)\gamma_2(k_x^2 + k_y^2 - 2k_z^2)$$

$$R_k = \left(\frac{\hbar^2}{2m_0}\right)\sqrt{3}[\gamma_2(k_x^2 - k_y^2) - 2i\gamma_3 k_x k_y]$$

$$S_k = \left(\frac{\hbar^2}{2m_0}\right)\sqrt{6}\gamma_3(k_x - ik_y)k_z$$

$$T_k = \frac{1}{\sqrt{6}}P_0(k_x + ik_y)$$

$$U_k = \frac{1}{\sqrt{3}}P_0 k_z$$

$$V_k = \left(\frac{\hbar^2}{2m_0}\right)\gamma_{Nc}(k_x^2 + k_y^2 + k_z^2).$$

Here, k_x, k_y, and k_z denote the components of the wave vector along the crystallographic directions [100], [010], and [001], respectively, $P_0 = -i(\hbar/m_0)\langle s_c|p_x|x\rangle$ $(E_P = 2m_0P_0^2/\hbar^2)$ is the Kane matrix element, γ_c, γ_1, γ_2, and γ_3, are modified Luttinger parameters related to the original Luttinger parameters (superscript L) and remote bands as $\gamma_c = 1/m_c^* - (E_P/3)\times[2/E_g + 1/(E_g + \Delta_{so})]$, $\gamma_1 = \gamma_1^L - E_P/(3E_g + \Delta_{so})$, and $\gamma_{2,3} = \gamma_{2,3}^L - E_P/(6E_g + 2\Delta_{so})$. Parameters γ_N and γ_{Nc} both vary at low nitrogen concentration as $x^{1/2}$ and can be estimated from

$$\left(\frac{\hbar^2}{2m_0}\right)\gamma_N k^2 = |\langle\Psi_N|H^{(At)}(k)|\Psi_N\rangle| - |\langle\Psi_N|H^{(At)}(\Gamma)|\Psi_N\rangle|$$

$$\left(\frac{\hbar^2}{2m_0}\right)\gamma_{Nc} k^2 = |\langle\Psi_N|H^{(At)}(k)|\Psi_c\rangle| - |\langle\Psi_N|H^{(At)}(\Gamma)|\Psi_c\rangle|,$$

where $H^{(At)}$ is an "atomistic" Hamiltonian expressed in the basis of individual atom orbitals.[35,36] In the flat nitrogen resonant band approximation, most commonly used in the literature $\gamma_N \to 0$. Adopting the argument[37] that the N wave function decays completely at the distance of the host material lattice constant, a_0, from the coherent potential approximation (CPA) it follows that $\gamma_{Nc} \to -(4m_0/\hbar^2)V_{Nc0}(x)a_0^2$, for $k^2 << 1/a_0^2$.

The strain dependent terms in the Hamiltonian Eq. (1) are given by:

$$N_\epsilon = +a_N(\epsilon_{xx} + \epsilon_{yy} + \epsilon_{zz})$$

$$O_\epsilon = +a_c(\epsilon_{xx} + \epsilon_{yy} + \epsilon_{zz})$$

$$P_\epsilon = -a_v(\epsilon_{xx} + \epsilon_{yy} + \epsilon_{zz})$$

$$Q_\epsilon = -\frac{b_v}{2}(\epsilon_{xx} + \epsilon_{yy} - 2\epsilon_{zz})$$

$$R_\epsilon = -\frac{\sqrt{3}}{2}b_v(\epsilon_{xx} - \epsilon_{yy}) + id_v\epsilon_{xy}$$

$$S_\epsilon = -\frac{d_v}{\sqrt{2}}(\epsilon_{zx} - i\epsilon_{yz})$$

$$T_\epsilon = \frac{1}{\sqrt{6}}P_0\sum_j(\epsilon_{xj} + i\epsilon_{yj})k_j$$

$$U_\epsilon = \frac{1}{\sqrt{3}}P_0\sum_j \epsilon_{zj}k_j$$

$$V_\epsilon = +a_{Nc}(\epsilon_{xx} + \epsilon_{yy} + \epsilon_{zz}),$$

where ϵ_{ij} are the strain tensor components, a_N is the nitrogen resonant band hydrostatic deformation potential, a_c and a_v are the conduction band and the valence band hydrostatic deformation potential of the host material, and b_v and d_v are the shear deformation potentials along [001] and [111] direction of the host material. From the comparison to the hydrostatic pressure experiment on the quantum well structures, we estimated the nitrogen level deformation potentials to vary with indium concentration y as $a_N \approx a_v + (0.21 - 0.08y)\times(a_c - a_v)$,[17,38] where a_c and a_v are the conduction and valence band deformation potential of the $In_yGa_{1-y}As$ host material, respectively. Because of a lack of information, we set $a_{Nc} = 0$ since its effect is already partially included in a_N.

Symmetry arguments indicate that the matrix elements

$$T_N = T_k^N + T_\epsilon^N$$

$$U_N = U_k^N + U_\epsilon^N$$

should vary linearly with k,

TABLE I. Material configurations of eight different $In_yGa_{1-y}As_{1-x}N_x/GaAs_{1-x^{mx}}N_{x^{mx}}$ dot-barrier systems analyzed in the text. y is the indium composition in the QD, x is the nitrogen composition in the QD, and x^{mx} is the nitrogen composition in the barrier region.

	(a)	(b)	(c)	(d)	(e)	(f)	(g)	(h)
y	1.0	0.5	0.5	0.5	0.7	0.7	0.7	0.7
x	0	0	0.02	0.02	0	0.02	0.02	0.04
x^{mx}	0	0	0	0.02	0	0	0.02	0

$$T_k^N = \frac{1}{\sqrt{6}} P_0^N (k_x + ik_y)$$

$$U_k^N = \frac{1}{\sqrt{3}} P_0^N k_z$$

$$T_\epsilon^N = \frac{1}{\sqrt{6}} P_0^N \sum_j (\epsilon_{xj} + i\epsilon_{yj}) k_j$$

$$U_\epsilon^N = \frac{1}{\sqrt{3}} P_0^N \sum_j \epsilon_{zj} k_j,$$

coupling the N level to the valence band, where $P_0^N = -i(\hbar/m_0)\langle s_N | p_x | x \rangle$. The atomistic-type calculations can provide a guide as to which are the most important parameters. The sp^3s^* TB calculations suggest that the dominant terms are those that are independent of k,[35] and included in Eq. (1) to describe the variation of the overall energy gap with N composition. Consequently, we set T_N and U_N to be zero.

The quantum dot breaks the translational symmetry along all three Cartesian directions, implying operator replacement $k_\nu \to -i\partial/\partial\nu$ in Eq. (1), where $\nu = x, y, z$. The material parameters for unperturbed InAs and GaAs crystals were taken from Ref. 21, while the lattice constant, elastic constants, and deformation potentials of zinc-blende GaN and InN are taken from Ref. 39. The whole Hamiltonian, $H = H_{\mathbf{k}} + H_{\mathbf{e}} + V_{pz}$, is expanded in the plane-wave basis set and directly diagonalzed by using ScaLAPACK and MPI packages on HPCx.[40] From non-self-consistent wave functions, we calculate the dimensionless scaled matrix element[21]

$$I_{[xyz]} = \left(\frac{\hbar}{m_0 P_0} \right)^2 |\hat{e} \cdot \mathbf{p}_{i,j}|^2, \tag{2}$$

where $\hat{e}$ is the light polarization vector and $\mathbf{p}_{i,j}$ is the momentum operator, and the Coulomb interaction energy

$$J_{i,j} = \frac{1}{4\pi\epsilon_0\epsilon_r} \int \int \frac{|\psi_i(\mathbf{r}_1)|^2 |\psi_j(\mathbf{r}_2)|^2}{|\mathbf{r}_1 - \mathbf{r}_2|} d\mathbf{r}_1 d\mathbf{r}_2 \tag{3}$$

between the CB and the VB states. The Kane matrix element P_0 and the dielectric permittivity ϵ_r are taken to be position independent and equal to the QD material values.

III. THE MODEL QUANTUM DOT

The model QD is a pyramid-shaped dot with a base length b of 20 lattice constants (11.3 nm) and a height $h = b/2$, on top of a one monolayer thick wetting layer (WL). Since the strain anisotropy and piezoelectric field are included the symmetry of the supercell is reduced to C_{2v}. The assumed temperature is $T = 0$ K. For an InAs/GaAs reference QD, our eight-band $\mathbf{k} \cdot \mathbf{p}$ model agrees very well, in terms of transition energies, with the $\mathbf{k} \cdot \mathbf{p}$ model when Keating-Martin valence force field (VFF) model of the strain, ignoring Cauchy violation in the elastic constants, is assumed,[21] and the agreement is also good in terms of $J_{ei,hj}$, $i, j \in (0, 1)$, Coulomb energies obtained by an atomistic method based on empirical pseudopotentials[26] (here systematically smaller by 0.5–1.1 meV).

To quantify the influence of the indium and nitrogen concentration on the band structure, eight different $In_yGa_{1-y}As_{1-x}N_x/GaAs_{1-x^{mx}}N_{x^{mx}}$-dot–barrier-material systems were compared to indium concentration in the dot region y, the nitrogen concentration in the dot region x, and the nitrogen concentration in the surrounding matrix region x^{mx} listed in Table I. Sample (a), InAs/GaAs is used as a reference and to validate the standard eight-band $\mathbf{k} \cdot \mathbf{p}$ model as mentioned above. The electronic structure of samples (a), (b), and (e) were then calculated by standard eight-band $\mathbf{k} \cdot \mathbf{p}$ model, while the properties of samples (c), (d), (f), (g), and (h) were calculated using the ten band $\mathbf{k} \cdot \mathbf{p}$ BAC Hamiltonian described in the Sec. II.

IV. RESULTS AND DISCUSSION

The reduction of the In content in the dot from pure InAs to $y = 50\%$, sample (b), significantly increases the energy gap of the dot material and reduces the lattice mismatch to 3.46%. The position of the conduction edge minima, $z = 0$, in the QD is at 1.225 (1.210) eV, (values in brackets are obtained assuming a homogeneous strain throughout the structure, $\epsilon_{zz} = -2\epsilon_{xx} c_{12}/c_{11}$, as in quantum wells, and are given for orientation), while the fundamental optical transition is $e0$-$h0 = 1.343$ eV, Fig. 1. Substitutional addition of the $x = 2\%$ of N in $In_{0.5}Ga_{0.5}As$ host material, sample (c), causes interaction between host material CB and the resonant N band via the BAC effect. This effect produces deepening of the CB offset in the QD of ~200 meV, improving the wavefunction confinement and increasing the Coulomb energy of the $e0$-$h0$ exciton by 2.3 meV. The BAC induces the new CB minimum at $E_- = 1.023$ (1.009) eV, reducing the optical transition energy to $e0$-$h0 = 1.236$ eV. A smaller lattice constant, due to the presence of the N atoms, further decreases the lattice mismatch to 3.07%. Compared to the N-free and $y = 50\%$ QD, sample (b), the dipole matrix element for the

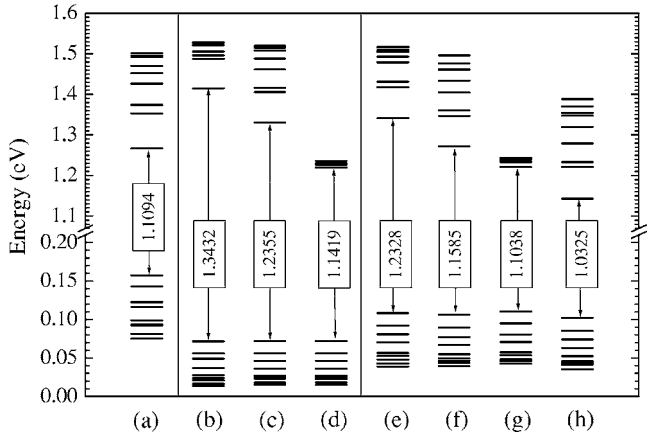

FIG. 1. The first nine energy levels in CB and VB of the 11.3 nm base and 5.6 nm height capped QD on 1 ML wetting layer: (a) InAs/GaAs, (b) $In_{0.5}Ga_{0.5}As/GaAs$, and (e) $In_{0.7}Ga_{0.3}As/GaAs$ dots calculated using the eight-band $\mathbf{k}\cdot\mathbf{p}$ method; (c) $In_{0.5}Ga_{0.5}As_{0.98}N_{0.02}/GaAs$, (d) $In_{0.5}Ga_{0.5}As_{0.98}N_{0.02}/GaAs_{0.98}N_{0.02}$, (f) $In_{0.7}Ga_{0.3}As_{0.98}N_{0.02}/GaAs$, (g) $In_{0.7}Ga_{0.3}As_{0.98}N_{0.02}/GaAs_{0.98}N_{0.02}$, and (h) $In_{0.7}Ga_{0.3}As_{0.96}N_{0.04}/GaAs$ dots calculated using ten-band $\mathbf{k}\cdot\mathbf{p}$ method. The values of $e0$-$h0$ transition energies are given in electron volts.

[100] polarization drops by ~43%, while the polarization anisotropy between $[1\bar{1}0]$ and [110] directions of the $e0$-$h0$ direct-transition is almost unchanged. The decreasing of optical dipole matrix element when N is added has previously been observed in the quantum well structures with a dilute amount of nitrogen.[29,41] In QDs with $y=50\%$ and $x=2\%$, a significant part (~34%) of the electron ground state belongs to the $|s_N\rangle$ character.

To quantify the influence of nitrogen on the band structure, we proceed the analysis with the set of samples [(e)–(h)], each of which has a different amount of nitrogen and the same In content of $y=70\%$ in the QD region. Figure 2 shows the band edge energies along the [001] direction of the three samples with different content of N in the QD: (a) $x=0$, (b) $x=2\%$, and (c) $x=4\%$. Because of dominant effects of BAC interaction and a reduced strain, the conduction band is strongly affected. The sample with $y=70\%$ and $x=4\%$ has an even deeper CB potential in the QD than the pure InAs/GaAs dot, inducing more tightly confined electron states. At the same time, a better confinement in the CB is achieved with significantly reduced lattice mismatch of 4.03% (6.68% in InAs/GaAs). The valence band structure is only slightly affected by nitrogen.

In detail, the increase of indium content to 70% and addition of $x=2\%$ of N in $In_{0.7}Ga_{0.3}As$ host material, sample (f), causes a smaller deepening (~150 meV) of the CB offset than in sample (c) with $y=50\%$ and $x=2\%$. This is explained in terms of a closer proximity of the CB host band and resonant N level and a stronger band mixing in the sample (c) with less indium[30] than in sample (f), which is also confirmed by a larger value of the nitrogen character of the $e0$ wave function[17] in the former: 0.342 vs 0.247, respectively (see Table II). This also suggests that it is possible to achieve the same energy of the fundamental transition with different (y,x) combinations regardless of the QD size, providing larger flexibility in device design.

To achieve a longer wavelength of the $e0$-$h0$ transition than in the sample with pure InAs QD, we study the sample with 4% of N in $In_{0.7}Ga_{0.3}As$, which we briefly discussed above. The character-decomposed electron and hole ground-state wave functions are given in Fig. 3. The electron ground state is composed predominantly of the s-like states, with a 31.7%/57.9% ratio between the nitrogen and host material conduction band character. The hole ground state is mostly of heavy hole character (81.2%) with negligible admixture of the nitrogen band (8.11×10^{-4} %). As expected, the effect of increased nitrogen concentration further increases the CB offset by ~280 meV relative to the corresponding N-free sample (e), Fig. 2(c). The CB minimum is at $E_-=0.787$ (0.772) eV, reducing the optical transition energy to $e0$-$h0$ = 1.033 eV, which is ~77 meV smaller than in pure InAs/GaAs QDs, sample (a). In contrast to the N-free and $y=70\%$ QD, the dipole matrix element for the [100] polarization drops by ~45%, and the polarization anisotropy is unchanged.

To illustrate the influence of nitrogen on the confinement, in Fig. 4 we compare the charge densities of the first few CB and VB states in the $y=70\%$ and N-free sample, against those in $y=70\%$ and $x=4\%$ QD. A stronger confinement of the first three states in the CB of $x=4\%$ QD is noticeable.

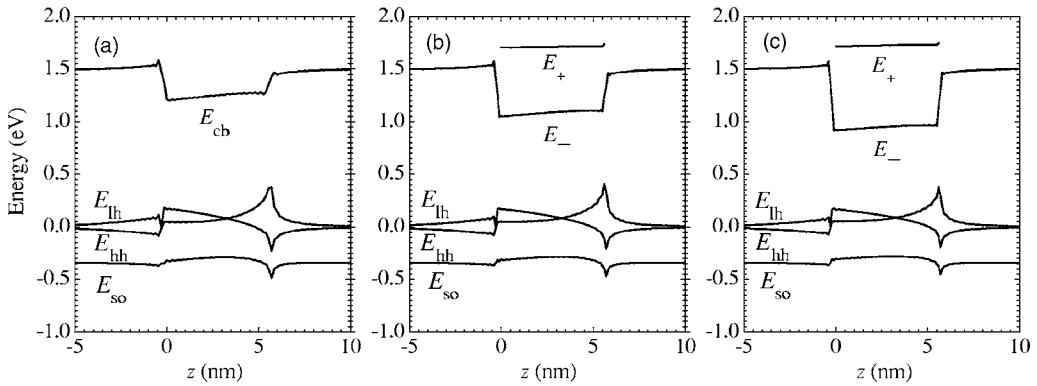

FIG. 2. Band structure along the [001] direction through the center of the QD for three samples with the same indium concentration, $y=70\%$, and different amounts of nitrogen: (a) N-free, (b) $x=2\%$, and (c) $x=4\%$.

TABLE II. The direct transition scaled matrix element $I_{[100]}$, the factor of electron ground-state anisotropy $I_{[1\bar{1}0]}/I_{[110]}$, the Coulomb interaction energy $J_{e0,h0}$ (in microelectron volts), and the character decomposition summed over both degenerate states.

	$I_{[100]}$	$I_{[1\bar{1}0]}/I_{[110]}$	$J_{e0,h0}$	$\lvert s_N\rangle/\lvert s_c\rangle/\lvert hh\rangle/\lvert lh\rangle/\lvert so\rangle$
(a)	0.107	1.62	27.2	0.891/0.031/0.053/0.025
(b)	0.147	1.35	27.9	0.920/0.023/0.037/0.020
(c)	0.084	1.36	30.2	0.342/0.586/0.020/0.035/0.017
(d)	0.014	1.34	10.2	0.361/0.636/0.001/0.001/0.001
(e)	0.128	1.47	28.8	0.897/0.029/0.049/0.025
(f)	0.083	1.49	29.5	0.247/0.668/0.024/0.041/0.020
(g)	0.054	1.47	18.6	0.302/0.676/0.007/0.010/0.005
(h)	0.071	1.47	30.8	0.317/0.579/0.030/0.051/0.023

Since the amplitude of nitrogen character $|s_N\rangle$ in dilute nitrogen heterostructures increases with increasing confinement energy,[17] an improved localization of higher states, $e1$ and $e2$, in $In_{0.7}Ga_{0.3}As_{0.96}N_{0.04}/GaAs$ QD is also visible. A slightly better confinement of the VB states in the N-free sample is attributed mainly to a stronger influence of strain.

Sample (d), with $x^{mx}=2\%$ of N added in the matrix material, mainly reflects the nature of the BAC in the barrier. In spite of further lowering of the $e0$-$h0$ transition energy when compared to the equivalent barrier N-free sample (c), the size-quantization effects for electrons are almost lost. The CB edge of the barrier is shifted down relative to the host GaAs due to BAC. This makes the CB potential for electrons almost flat (Fig. 5). In addition, the electron effective mass in the barrier is larger than in the QD region,[18] providing only weak "confinement by effective mass." The first electron state is very much delocalized (Fig. 6). The CB character of $e0$ is mostly localized in the QD while the nitrogen character is spread into the surrounding material due to the continuity of the nitrogen band over the QD/barrier interface. To account for this effect, we made an estimate based on simplified two component electron wave functions, taking into account only the influence of the nitrogen and host conduction band.[17] The wave functions are assumed in the form

$$\Psi^{qd} = \begin{pmatrix} \alpha_N \\ \alpha_c \end{pmatrix} f(\mathbf{r}) \text{ and } \Psi^{mx} = \begin{pmatrix} \beta_N \\ \beta_c \end{pmatrix} g(\mathbf{r}) \tag{4}$$

in the QD and in the barrier region respectively, where $g(\mathbf{r}) \sim \exp(-\kappa \mathbf{r})$. The effect of the ground-state wave function "leakage," and the $|s_N\rangle$ character localization in the surrounding matrix material while $|s_c\rangle$ is still localized inside the QD, might both be surprising at first sight. This situation corresponds to the ratio between different wave-function amplitudes when $\beta_N/\beta_c > \alpha_N/\alpha_c$. Indeed, for sample (d): $\beta_N/\beta_c \sim 0.8$ and $\alpha_N/\alpha_c \sim 0.5$. Actually, in the upper part of the QD, where electrons are predominantly localized, $\kappa \in \Re$ is not fulfilled until $z > 4$ nm above the QD apex. The same tendency is observed in sample (g), although the increased indium content provides slightly better confinement for electrons. The effect of delocalization is also reflected to a rapid decrease of the $I_{[100]}$, see Table II. Nevertheless, about one third of the wave function is still on the $|s_N\rangle$ site.

Finally, we briefly discuss the influence of quantum size effects on the $e0$-$h0$ transition energy of QDs. Figure 7 shows the variation of the $e0$-$h0$ transition energy in the $In_{0.7}Ga_{0.3}As_{0.96}N_{0.04}/GaAs$ QDs when the pyramid base

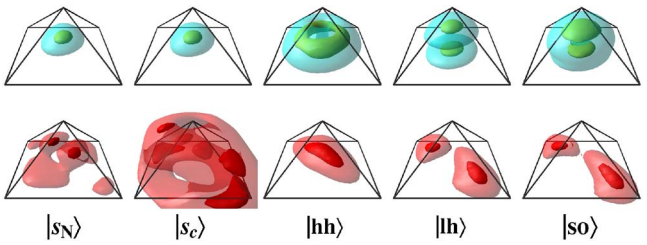

FIG. 3. (Color online) Decomposition of the electron (top row) and hole (bottom row) ground-state wave function of the $In_{0.7}Ga_{0.3}As_{0.96}N_{0.04}/GaAs$ QD into their basis states, as described in the text. Surface plots are at the 25% (transparent) and 75% of the maximum charge density. Electron wave function is mainly of s-like characters (89.6%), the $|hh\rangle$ is clearly a linear combination of p_x and p_y orbitals, while in $|lh\rangle$ and $|so\rangle$ are expressive p_z aspect. The VB ground state is mostly $|hh\rangle$ and $|lh\rangle$ in character, 81.2% and 16.8%, respectively, with just 1.6% of $|so\rangle$, 0.3% of $|s_c\rangle$, and a negligible 8.11×10^{-4} % of $|s_N\rangle$.

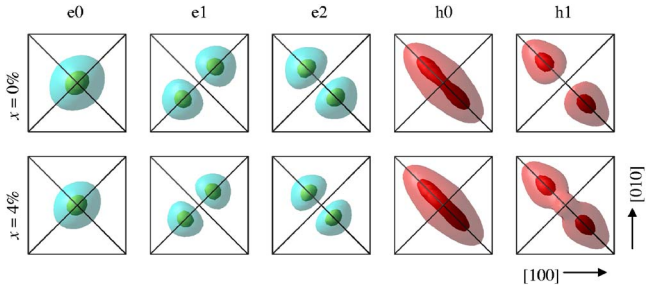

FIG. 4. (Color online) The wave-function square of the three lowest CB and two highest VB states in (top row) N-free $In_{0.7}Ga_{0.3}As/GaAs$ QD and (bottom row) $In_{0.7}Ga_{0.3}As_{0.96}N_{0.04}/GaAs$ QD. Isosurfaces are plotted at 25% (transparent) and 75% of the maximum charge density. A better electron confinement is noticeable in the sample with $x=4\%$.

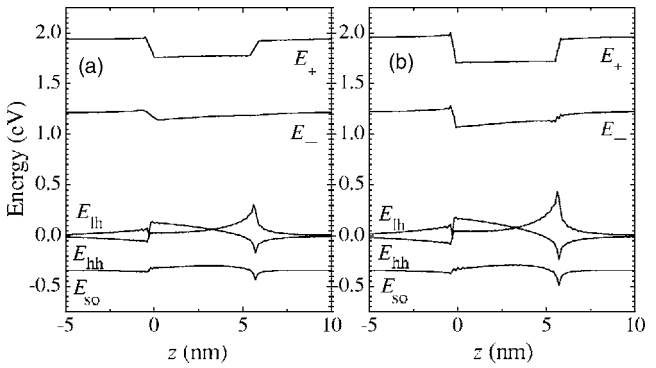

FIG. 5. Band structure along the [001] direction through the center of the QD for two samples with the same nitrogen concentration in the QD and barrier region, $x=x^{mx}=2\%$, and different amounts of indium in the QD: (a) $y=50\%$ and (b) $y=70\%$.

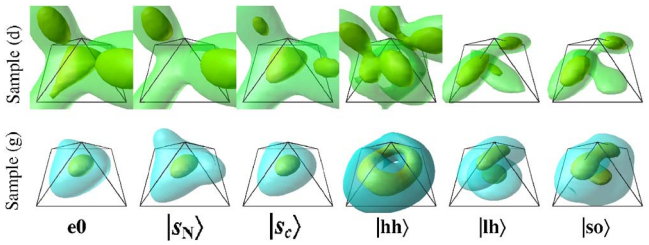

FIG. 6. (Color online) Spatial decomposition of the electron ground-state wave-function square into its basis states summed over both spins: (top row) $In_{0.5}Ga_{0.5}As_{0.98}N_{0.02}/GaAs_{0.98}N_{0.02}$ QD where, due to strong delocalization, the surface plots are at 50% (transparent) and 75%, and (bottom row) $In_{0.7}Ga_{0.3}As_{0.98}N_{0.02}/GaAs_{0.98}N_{0.02}$ QD, where the surface plots are at 25% (transparent) and 75% of the maximal charge density. The $|hh\rangle$, $|lh\rangle$, and $|so\rangle$ stands for $|u_3\rangle$, $|u_4\rangle$, and $|u_5\rangle$ characters, respectively, as described in the text. The tendency of $|s_N\rangle$ character "leakage" into the barrier region is visible in both samples.

length is changed from 20 to 36 lattice constants of GaAs. The corresponding dependence in pure InAs/GaAs QDs is also given, for purpose of comparison. For the largest (b =20.4 nm) QD with x=4%, the $e0$-$h0$ transition energy is estimated to be 0.894 eV ($\sim$1.39 μm), while its Coulomb energy is 15 meV. At room temperature, the emission moves further toward longer wavelengths. However, the shift will be smaller than in the bulk III-V, because the dilute nitride and the QD structure itself both reduce the E_g temperature sensitivity.

By comparing our theoretical results to experimental findings we observe: (i) for y=70% and x=4% QD samples grown at 520 °C [which results in $h\sim8$ nm ($b\sim16$ nm)][7] the PL wavelength is 1.27 μm, while we predict the wavelength of 1.32 μm for the same (y,x) and b=30a (17 nm); (ii) the reported dependence of measured wavelengths (in the range from 1.28 μm to 1.45 μm at T=10 K)[7] on the growth temperature (QD size) is in good agreement with theoretical predictions for direct transition wavelengths (1.2–1.39 μm), having in mind the uncertainty of the QD size, shape, and In and N profiles; (iii) for the sample with y=70%, x=2% and lateral dot dimension of 15 nm, the measured micro-PL is 1.15 μm (1.08 eV),[8] which is in Fig. 7, halfway between the N-free and x=4% lines for the similar QD size; and (iv) the theoretical results for samples (d) and (g), with the N in the barrier region, can partly explain the observed increase of the emission wavelength and a radical lowering of the PL emission intensity with increased N concentration in the capped layer above the QD,[11] due to weakened quantum size effects and strong degradation of the confinement ability, respectively.

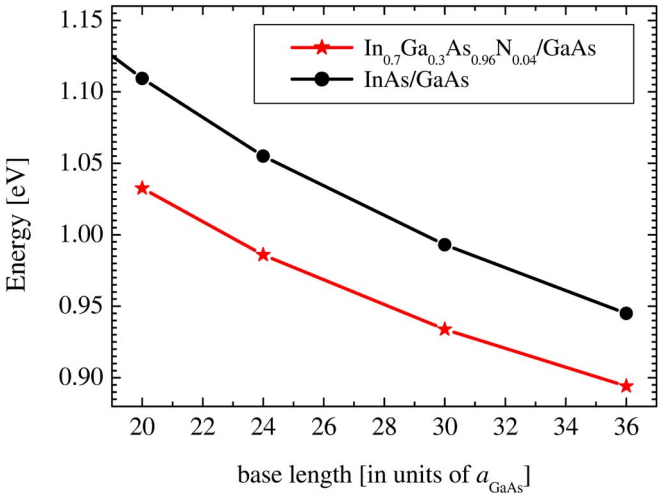

FIG. 7. (Color online) Transition energy between QD electron and hole ground states as a function of dot size at T=0 K: (●) InAs/GaAs QD's and (⋆) $In_{0.7}Ga_{0.3}As_{0.96}N_{0.04}/GaAs$ QDs.

V. CONCLUSIONS

In summary, we have presented a theoretical analysis of ideal dilute nitrogen InGaAsN/GaAs(N). Our analysis shows that the presence of nitrogen induces more confined states in the CB than in equivalent N-free QDs, reducing the energy of the fundamental optical transition. The better confinement in dilute nitrogen QD is due to both a significantly reduced compressive strain, which was one of the major obstacles for a long-wavelength emission from InAs/GaAs QDs, and to the BAC effect. These effects, in conjunction with QD size variation, can be of great benefit for the design of devices emitting at longer wavelengths. Furthermore, in contrast to N-free QDs, dilute nitrogen QDs exhibit a reduced dipole matrix element and a larger Coulomb interaction energy. Our findings are in good agreement with the reported experimental results on similar structures. We conclude that several possible routes toward the 1.55 μm wavelength emission would be a further increase of the indium content in nitrogen reach ($x\sim4\%$) QD, an increase of the QD size/volume, or vertically aligned and coupled dilute nitrogen QDs.

ACKNOWLEDGMENTS

The author is grateful to the Engineering and Physical Sciences Research Council (EPSRC) UK and the CCP3 Consortium for supporting this work. I wish to thank I. J. Bush, Z. Ikonić, T. S. Jones, P. J. Klar, E. P. O'Reilly, B. G. Searle, A. G. Sunderland, and M. Tadić for useful discussions.

[1] A. A. Ukhanov, A. Stintz, P. G. Eliseev, and K. J. Malloy, Appl. Phys. Lett. **84**, 1058 (2004).
[2] T. Akiyama, N. Hatori, Y. Nakata, H. Ebe, and M. Sugawara, Electron. Lett. **38**, 1139 (2002).
[3] A. V. Uskov, E. P. O'Reilly, D. McPeake, N. N. Ledentsov, D. Bimberg, and G. Huyet, Appl. Phys. Lett. **84**, 272 (2004).
[4] Z. Yuan, B. E. Kardynal, R. M. Stevenson, A. J. Shields, C. J. Lobo, K. Cooper, N. S. Beattie, D. A. Ritchie, and M. Pepper, Science **295**, 102 (2002).
[5] G. Bester, A. Zunger, and J. Shumway, Phys. Rev. B **71**, 075325 (2005).
[6] C. W. Tu, in *Physics and Applications of Dilute Nitrides*, edited by I. A. Buyanova and W. M. Chen (Taylor & Francis, New York, 2004), pp. 281–307.
[7] M. Sopanen, H. P. Xin, and C. W. Tu, Appl. Phys. Lett. **76**, 994 (2000).
[8] A. Nishikawa, R. Katayama, K. Onabe, Y. G. Hong, and C. W. Tu, J. Cryst. Growth **278**, 244 (2005).
[9] R. Oshima and Y. Okada, Thin Solid Films **464–465**, 229 (2004).
[10] K. C. Yew, S. F. Yoon, and Z. Z. Sun, J. Cryst. Growth **271**, 8 (2004).
[11] O. Schumann, S. Birner, M. Baudach, L. Geelhaar, H. Eisele, L. Ivanova, R. Timm, A. Lenz, S. K. Becker, M. Povolotskyi, M. Dähne, G. Abstreiter, and H. Riechert, Phys. Rev. B **71**, 245316 (2005).
[12] W. Shan, W. Walukiewicz, J. W. Ager III, E. E. Haller, J. F. Geisz, D. J. Friedman, J. M. Olson, and S. R. Kurtz, Phys. Rev. Lett. **82**, 1221 (1999).
[13] R. Fehse, S. Tomić, A. R. Adams, S. J. Sweeney, E. P. O'Reilly, A. Andreev, and H. Riechert, IEEE J. Sel. Top. Quantum Electron. **8**, 801 (2002).
[14] C. G. Van de Walle, Phys. Rev. B **39**, 1871 (1989).
[15] P. R. C. Kent and A. Zunger, Phys. Rev. Lett. **86**, 2613 (2001).
[16] A. Lindsay and E. P. O'Reilly, Phys. Rev. Lett. **93**, 196402 (2004).
[17] S. Tomić, E. P. O'Reilly, P. J. Klar, H. Grüning, W. Heimbrodt, W. M. Chen, and I. A. Buyanova, Phys. Rev. B **69**, 245305 (2004).
[18] S. Tomić and E. P. O'Reilly, Phys. Rev. B **71**, 233301 (2005).
[19] M. A. Cusack, P. R. Briddon, and M. Jaros, Phys. Rev. B **54**, R2300 (1996).
[20] C. Pryor, Phys. Rev. B **57**, 7190 (1998).
[21] O. Stier, M. Grundmann, and D. Bimberg, Phys. Rev. B **59**, 5688 (1999).
[22] A. D. Andreev and E. P. O'Reilly, Phys. Rev. B **62**, 15851 (2000).
[23] V. Mlinar, M. Tadić, B. Partoens, and F. M. Peeters, Phys. Rev. B **71**, 205305 (2005).
[24] W. Sheng, S.-J. Cheng, and P. Hawrylak, Phys. Rev. B **71**, 035316 (2005).
[25] A. Zunger, MRS Bull. **23**, 35 (1998).
[26] L. W. Wang, J. Kim, and A. Zunger, Phys. Rev. B **59**, 5678 (1999).
[27] L.-W. Wang and A. Zunger, Phys. Rev. B **59**, 15806 (1999).
[28] A. Canning, L. W. Wang, A. Williamson, and A. Zunger, J. Comput. Phys. **160**, 29 (2000).
[29] S. Tomić, E. P. O'Reilly, R. Fehse, S. J. Sweeney, A. R. Adams, A. D. Andreev, S. A. Choulis, T. J. C. Hosea, and H. Riechert, IEEE J. Sel. Top. Quantum Electron. **9**, 1228 (2003).
[30] P. J. Klar, H. Grüning, J. Koch, S. Schäfer, K. Volz, W. Stolz, W. Heimbrodt, A. M. Kamal-Saadi, A. Lindsay, and E. P. O'Reilly, Phys. Rev. B **64**, 121203(R) (2001).
[31] M. Hetterich, A. Grau, A. Yu. Egorov, and H. Riechert, J. Appl. Phys. **94**, 1810 (2003).
[32] A. Lindsay and E. P. O'Reilly, Physica B **340–342**, 434 (2003).
[33] M. Grundmann, O. Stier, and D. Bimberg, Phys. Rev. B **52**, 11969 (1995).
[34] A. D. Andreev, J. R. Downes, D. A. Faux, and E. P. O'Reilly, J. Appl. Phys. **86**, 297 (1999).
[35] E. P. O'Reilly, A. Lindsay, S. Tomić, and M. Kamal-Saadi, Semicond. Sci. Technol. **17**, 870 (2002).
[36] M. Cardona, N. E. Christensen, and G. Fasol, Phys. Rev. B **38**, 1806 (1988).
[37] J. Wu, W. Walukiewicz, and E. E. Haller, Phys. Rev. B **65**, 233210 (2002).
[38] S. A. Choulis, T. J. C. Hosea, S. Tomić, M. Kamal-Saadi, A. R. Adams, E. P. O'Reilly, B. A. Weinstein, and P. J. Klar, Phys. Rev. B **66**, 165321 (2002).
[39] I. Vurgaftman and J. R. Meyer, J. Appl. Phys. **94**, 3675 (2003).
[40] http://www.hpcx.ac.uk
[41] M. Geddo, R. Pezzuto, M. Capizzi, A. Polimeni, D. Gollub, M. Fischer, and A. Forchel, Eur. Phys. J. B **30**, 39 (2002).